DOI: 10.1002/ ((please add manuscript number))

**Article type (Full paper)**

# Title: Circumventing UV light induced nano-morphology disorder to achieve long lifetime PTB7-Th:PCBM based solar cells

Quan Liu[1], Johann Toudert[1], Feng Liu[2,3], Paola Mantilla-Perez[1], Miguel Montes Bajo[1], Thomas P. Russell[4] and Jordi Martorell[1,5]*

**Affiliations**

[1]ICFO-Institut de Ciencies Fotoniques, The Barcelona Institute of Science and Technology, 08860 Castelldefels (Barcelona), Spain

[2]Materials Sciences Division, Lawrence Berkeley National Laboratory, Berkeley, California 94720, USA

[3]Department of Physics and Astronomy, Shanghai Jiao Tong University, Shanghai 200240, P. R. China

[4]Department of Polymer Science and Engineering, University of Massachusetts, Amherst, Massachusetts 01003, USA

[5]Departament de Física, Universitat Politècnica de Catalunya, 08222 Terrassa, Spain

*Corresponding author e-mail: jordi.martorell@icfo.es

**Keywords:** Organic photovoltaics, photostability, PCBM, PTB7-Th, Burn-in

**Abstract**

Large area flexible electronics rely on organic or hybrid materials prone to degradation limiting the device lifetime. For many years, photo-oxidation has been thought to be one of the major degradation pathways. However, intense illumination may lead to a burn-in or a rapid decrease in performance for devices completely isolated from corrosive elements as oxygen or moisture. The experimental studies we present in here indicate that a plausible triggering for the burn-in is a spin flip after a UV photon absorption leading to the accumulation of electrostatic potential energy that initiates a rapid destruction of the nano-morpholgy in the fullerene phase of a polymer cell. To circumvent this and achieve highly stable and efficient devices, we induce a robust nano-crystalline ordering in the PCBM phase prior to UV illumination. In that event, PTB7-Th:$PC_{71}BM$ cells are shown to exhibit $T_{80}$ lifetimes larger than 1.6 years under a continuous UV-filtered 1-sun illumination, equivalent to 7 years for sunlight harvesting at optimal orientation and 10 years for vertical applications.

## 1. Introduction

Solution-processed electronic devices based on organic or hybrid materials already exhibit a high performance level that can surpasses their inorganic counterparts. Besides low cost production, hybrid electronics may offer a high degree of flexibility which makes them useful in many applications where the inherent rigidity of inorganic materials is not suitable. Good examples are semi-transparent, bendable or portable smart optoelectronic devices, and flexible or semi-transparent photovoltaic solar cells. Yet, a limited durability or a short-term stability remains as the Achilles heel for such technology.[1]

Fullerenes or their solution processable PCBM derivatives are the standard electron acceptors in organic solar cells (OSCs)[2-4] and their use as the electron transporter in inverted perovskite solar cells recently consolidated when record performing semi-transparent cells forming a tandem with lower band gap absorbers such as Si or Copper indium gallium selenide (CIGS) were demonstrated.[5,6] They are also used in polymer photodetectors,[7] biosensors,[8] or in organic light emitting diodes.[9,10] For the most studied case of OSCs, different experimental results has demonstrated that the rapid decrease in device performance when exposed to light, known as burn-in,[11] can be linked to a rapid degradation of the electron transport, while the transport of holes appears to be unaffected.[12] This burn-in is thought to lead to a degradation of the morphology of the blend,[13,14] to the formation of trapped states,[15] or to a broadening of the density of states,[16] or to form persistent free radicals in fullerene derivatives. [17] These effects have been shown to reduce the short-circuit current ($J_{sc}$)[18] and other photovoltaic (PV) parameters, like the open-circuit voltage ($V_{oc}$).[16,19]

When organic or Perovskite devices are isolated form aggressive corrosive agents, such as oxygen or moisture, the major source of cell degradation rests with ultraviolet (UV) photon

exposure.[20-22] Indeed, a short exposure to UV photons is sufficient to induce for some devices a decrease in efficiency close to 50%.[11,23] Even though UV radiation has been demonstrated to cause photooxidative degradation,[24] negligible changes in the absorption spectrum are observed when such photoactive material is illuminated in the absence of oxygen.[25] The degradation dynamics directly linked to the absorption of UV photons, which in the absence of any oxidative elements leads to a dramatic irreversible change in the nano-morphology of the fullerene acceptor phase is still not known. Understanding why the absorption of low momentum particles leads to a major material reorganization is essential to circumvent this problem.

In the current work, we demonstrate that the degradation dynamics is intrinsic to the absorption of UV photons in the [6,6]-Phenyl $C_{71}$-butyric acid methyl ester ($PC_{71}BM$) acceptor phase and a subsequent spin flip at the $PC_{71}BM$/active layer interface leading to the formation of $PC_{71}BM$ triplet anions and the accumulation of electrostatic potential energy. The release of this electrostatic potential energy in excess carries out a destruction of a weakly bonded nanomorphological order. Understanding this allowed us to implement the path to channel such electrostatic energy to prevent the destruction of the $PC_{71}BM$ nanomorphology. Prior to UV illumination we introduced a high degree of nanocrystalline ordering in the electron transporter to ease charge transport leading to very stable devices with high power conversion efficiencies (PCEs).

## 2. Results and discussion

### 2.1 Light-induced burn-in in polymer solar cells

In this paper, we consider cells where the active material is a blend of the high performance polymer Poly[4,8-bis(5-(2-ethylhexyl)thiophen-2-yl)benzo[1,2-b;4,5-b']dithiophene-2,6-diyl-

alt-(4-(2-ethylhexyl)-3-fluorothieno[3,4-b]thiophene-)-2-carboxylate-2-6-diyl)] (PTB7-Th) and the fullerene derivative $PC_{71}BM$ mixed in a 1:1.5 weight ratio. Such blend is well dissolved in the chlorobenzene (CB) and 3 vol% 1,8 diiodooctane (DIO) binary solvent. This solution is used to spin-coat a thin active layer in an inverted cell configuration (shown in **Figure 1**a), used as a reference throughout the text, that has a morphology comprised of nanoscopic domains of each component.[26,27] This final nanomorphology is essential to reach the highest possible efficiency.[28-30] Within each nanodomain there is a certain degree of crystalline order to facilitate the charge transfer to the corresponding electrode.[31,32] At the interface between the two components, excitons generated by photon absorption are separated into electrons and holes. Excitons are generated in both the donor and acceptor phases. Photon absorption at the $PC_{71}BM$ phase peaks at 470, 380 and below 300 nm. In a recent measurement of the $PC_{71}BM$ photoluminescence at 5K, performed by Dyakonov and co-workers,[33] the $S_1$ to $S_0$, $T_1$ to $S_0$, and $T_2$ to $T_1$ transitions were identified to be at 710, 800, and 900 nm, respectively. The estimated positions of these levels in an energy diagram are indicated in **Figure 1**b. Note that the exact $S_2$ to $S_0$ transition energy is not known and $S_2$ is pictured with an undefined position in the energy level diagram in **Figure. 1**b. After diffusion, excitons created in the $PC_{71}BM$ phase reach the PTB7-Th/$PC_{71}BM$ interface and access an intermolecular charge transfer (CT) state. In the CT state the binding energy is reduced and excitons are prone to dissociate.[34,35] Depending on the absorbed photon energy, the CT states may be of $S_2$ or $S_1$ type. A larger electron-hole separation for the $S_2$ type CT state results in an even weaker binding energy, which combined with a similar energy for the $S_2$ and $T_2$ levels, provides an effective path for a spin flip to occur. Because of a forbidden $T_1$ to $S_0$ transition the $PC_{71}BM$ anion of triplet type will live longer than an equivalent one of singlet type. A repulsive Coulombic interaction among several of such long-lived anions will favor a destruction of the order in the acceptor phase. Indeed, a continuous illumination with UV

photons leads to a rapid escalation in and irreversible destruction of the acceptor phase order, as schematically shown in **Figure. 1**c. The electrostatic potential energy that is accumulated in the acceptor phase cannot be easily channeled to the cathode when the anions are of triplet character, causing a stress in the blend morphology. Blends with a higher degree of crystallinity are more likely to withstand the pressure to release such electrostatic potential energy.

### 2.2 UV-Induced Degradation of Exciton Diffusion and Charge Mobility in $PC_{71}BM$ Nano Domains

To confirm that the degradation dynamics is triggered by the UV photon absorption, we studied the evolution of the PV parameters from encapsulated cells subject to a filtered 1-sun illumination. We used different UV longpass filters with cut-off wavelengths at 455, 400, 370 and 320 nm. As seen in **Figure. 2**a and Figure S1, when the 320 nm cut-off filter or no UV filter were applied, the $J_{sc}$, $V_{oc}$ and fill factor (FF) degraded, being the $J_{sc}$ the parameter that exhibited the strongest decay. In contrast, when UV photons below 370 nm were filtered, $V_{oc}$ was shown to be very stable during aging, while both $J_{sc}$ and FF dominated the degradation process. All the the normalized PCE evolutions can be adjusted to a double exponential decay with one large and one small time constant. All time constants and amplitudes used to fit the data are given in Table S1 in the Support Information. When the amplitude ($A_1$) corresponding to the short time exponential decay, which is directly linked to the burn-in, is plotted against the cut-off filter wavelength, as shown in Figure. 1a, one observes a sharp transition occurring between 320 and 370 nm. This links the burn-in degradation threshold to transitions from the ground state to higher electronic states beyond the $S_0$ to $S_1$ electronic transition. As indicated above, when the higher energy exctions are in the CT state, a spin flip is more likely to occur leading to the formation of $PC_{71}BM$ triplet anions. The expected

longer lifetimes for such triplet anions are confirmed in a time-resolved transient absorption experiment probing a 100 nm reference blend film deposited on fused silica glass substrate. The experimental setup is shown in Figure S2 in the Support Information and details of the transient absorption measurements are given in the Supporting Information. This layer is probed using a 765 nm 120 fs pulse and pumped either with a pulse at the same wavelength or its second harmonic at 382.5 nm. As shown in **Figure. 2**b, when the layer is pumped with the UV pulse at 382.5 nm, normalized absorption of the probe decreases if the probe and pump pulses overlap and remains unchanged, even when the probe pulse is delayed to the maximum time allowed by the setup. On the contrary, when a device is pumped with an infrared pulse tuned at 765 nm, we observe an ≈200 ps time constant decay which is close to the typical nano or sub nanosecond time constant decays seen in the allowed singlet to singlet molecular transitions.

The destruction of the order in the acceptor phase can be visualized in the external quantum efficiency (EQE) spectra as well as in single-polar devices. After aging the cells for 150 hours of non-UV-filtered AM1.5G 1-sun illumination, the EQE shown in the inset of Figure 2c exhibits a large reduction in the side of the $PC_{71}BM$ absorption band (300–550 nm) while the side of the PTB7-Th absorption band (550–800 nm) remains relatively unchanged. These relative differences in the normalized EQE, seen in Figure 2c, clearly indicate that exciton diffusion in the $PC_{71}BM$ phase is severely hindered provided that no change in the absorption wavelength dependence is seen (Figure S3, Supporting Informaion). In other words, in the degraded cell, excitons created in the accepter phase have more difficulties in reaching the interface. Electron-only devices fabricated from the reference active blends, indicate a dramatically diminished electron mobility with respect to light aging time, as shown in Figure 2d. The electron mobility measured by the space-charge-limited current method (SCLC) was

decreased by four orders of magnitude after 45 h of AM 1.5G non-UV-filtered 1-sun illumination, from $2.43 \times 10^{-3}$ to $2.16 \times 10^{-7}$ $cm^2$ $V^{-1}$ $s^{-1}$. In contrast, the transport of holes in PTB7-Th phase was slightly reduced by less than one order of magnitude (Figure S4a, Supporting Information). Note that such fast degradation in electron mobility can be greatly alleviated by filtering UV photons, as seen in Figure S4b in the Supporting Information, confirming that UV-induced disruption of the electron transport channel in the $PC_{71}BM$ phase is the primary source of burn-in triggering. Note that, contrary to what happens with $PC_{60}BM$ based photovoltaic cells,[36-38] there is no evidence of $PC_{71}BM$ fullerene dimerization[39-41] after light-soaking, which is confirmed by the transmittance and Raman spectra comparing fresh and light-aged $PC_{71}BM$ samples (see Figure S5 in the Supporting Information).

The transfer of the photon energy to a CT state of triplet character is intrinsic to the acceptor phase at the donor-acceptor interface. However, once the energy has been converted into electrical potential energy the acceptor phase morphology, as well as the surrounding environment, play a fundamental role in the degradation of the electrical performance of the OSC. Consequently, using the same acceptor, $PC_{71}BM$, but a different donor polymer, results in a second stage of degradation that is markedly different in the UV light-induced aging.[15] The relevant role played by the acceptor environment was recently confirmed when the burn-in was reduced by confining the acceptor domains in between polymer domains of increased crystallinity[39] or with higher molecular weight polymer chains.[42]

### 2.3 Circumventing PCBM Disorder to Achieve Highly Stable Cells with High Efficiency

To circumvent such powerful UV-induced $PC_{71}BM$ disorder without having to replace PTB7-Th by a less efficient PV polymer that would better confine or immobilize the $PC_{71}BM$ molecules, one must implement a set of procedures to freeze-in the morphological order in the

blend, particularly in the acceptor domains. In addition to an obvious filtering of high energy photons, measures must be taken to limit the $PC_{71}BM$ anion mobility. The use of DIO was eliminated since this additive may promote the penetration of $PC_{71}BM$ into the polymer domains, thus facilitating the acceptor morphological disorder.[14,43] We also eliminated other oxidant sources, such as the ZnO buffer layer, which may accelerate the degradation dynamics,[35] and we applied a thermal annealing, prior to light soaking, to increase the active layer crystalline order, particularly, in the $PC_{71}BM$ domains.

The latter treatment combined with the absence of DIO requires an optimization of the blend composition. Cells prepared without DIO were fabricated with PTB7-Th:$PC_{71}BM$ blends using 1,2-dichlorobenzene (DCB) as the solvent and Poly[(9,9-bis(3'-(N,N-dimethylamino)propyl)-2,7-fluorene)-alt-2,7-(9,9-dioctylfluorene)] (PFN) is electron-transporting layer (ETL) (hereafter referred as DIO-free cells). Using the donor/acceptor weight ratio of 1:1.5 of the reference cells, the DIO-free cells exhibited an inferior performance with the PCE and FF averaging 7.82% and 65%, respectively. By increasing $PC_{71}BM$ loading in the blends, an optimal performance for such DIO-free cells was obtained for a 1:2.0 weight ratio which had a best PCE of 9.6%, as seen in **Figure 3**a and Table S2 in the Supporting Information, where detailed PV parameters are given. The improved FF and $J_{sc}$ in higher $PC_{71}BM$ fraction blends should be ascribed to the increased donor/acceptor interface area and the formation of ideal electron transporting channels. As shown in Figure 3b, when a thermal annealing is applied on the completed cells, DIO-free cells exhibited excellent short-circuit current stability. In contrast, a 10% $J_{sc}$ drop was observed in the DIO cells, which was confirmed by the evolution of the EQE under this treatment (as shown in Supporting Information Figure S6). We observe for thermally treated DIO-free a small wavelength-independent reduction in the EQE, while a larger decrease in 340–450 nm

$PC_{71}BM$ region can be found in EQE of the reference devices. DIO-free cells also show an improved FF and PCE stability relative to reference blends, shown in Figure S7 in the Support Information, and a more stable blend nanomorphology as seen in the AFM images in Figure S8.[44] Note that the reference cell, when using SG-ZnO as ETL exhibited a large ~30% reduction in $J_{sc,}$ when the a thermal annealing is applied only for a short period of time. When the annealing is applied for 25 hours, such reference cells are stabilized with just a 10% reduction in $J_{sc,}$. Why there is such a large difference between the short and long annealing for the reference cell remains unclear, but the better performance of a reference cell fabricated with PFN instead of SG-ZnO may be ascribed to a stronger molecular interaction between PFN and $PC_{71}BM$, which limits the mobility of $PC_{71}BM$ molecules during the annealing process.

When considering the DIO-free cells, we observe, as shown in Figure 3c and **Table 1**, a decreasing sensitivity to light stress as the time for thermal annealing is increased. For the longest 25 hour annealing time, the PCE versus light soaking time dynamics can be adjusted to a single exponential, indicating an almost complete elimination of the burn-in degradation. Indeed, the amplitude $A_1$ for the fast exponential decay was reduced by more than one order of magnitude. For the PFN-reference cells we observed a similar trend when considering the normalized PCE degradation evolution under light soaking at different annealing times, as can be seen in **Figure 3**d (other PV parameter evolutions are also shown in Figure S9 in the Supporting Information). This clearly indicates that the thermal annealing is directly acting on the blend rather than on any of the buffer layers. It is worth noting that after the optimal thermal treatment, both PFN-reference cells and DIO-free cells show very stable $V_{oc}$ even under full sun illumination and FF dominates the decay process, indicating that UV light

induced $PC_{71}BM$ phase disorder has been suppressed and interfacial degradation may become dominating.

To gain insight into the $PC_{71}BM$ nano-morphology order with respect to thermal annealing, we performed grazing incidence wide-angle X-ray diffraction (GIXD) measurements on the blend films.[45,46] The two-dimensional GIXD patterns of DIO-free blend film prior and after the 25 h thermal annealing are shown in **Figure 4**a and **4**b, respectively. The as-cast blend film exhibited a diffuse diffraction arc at q = 1.35 $Å^{-1}$ with no azimuthal dependence, which suggested that the $PC_{71}BM$, if crystalline, were poorly ordered and randomly oriented.[40,47] After 25 h thermal annealing, an intense diffraction arc was visible over the whole $PC_{71}BM$ region, indicative of a high degree of $PC_{71}BM$ crystalline ordering. A similar behavior was seen in the PFN reference blend films as shown in Figure S10 of the Supporting Information. To quantify the level of order achieved, we considered, the in-plane and out-of-plane line cuts, show in **Figure 4**c, and a multi-peak fitting to analyze the diffraction in the 0.9–2.2 $Å^{-1}$ region (See Figure S11in the Support Information). A weak reflection peak (010) observed at around 1.61 $Å^{-1}$ in the out-of-plane direction corresponds to the PTB7-Th polymer $\pi$-$\pi$ stacking. As seen in Figure S11 in the Supporting Information, no change was observed in the full width at half-maximum for either the $PC_{71}BM$ or the PTB7-Th, indicating that their respective crystal sizes did not change after the thermal treatment. However, the relative peak areas of $PC_{71}BM$ (q = 1.35 $Å^{-1}$ and q = 1.89 $Å^{-1}$) in the out-of-plane direction significantly increased suggesting an increase in $PC_{71}BM$ ordering in the annealed blends. It is worth noting that a more pronounced PTB7-Th (100) peak was seen in the in-plane direction at 0.3 $Å^{-1}$ (Figure 4c), indicating a large number of face-on oriented crystals in the annealed sample. Moreover, a slight increase in the out-of-plane PTB7-Th (010) peak relative area was also observed after thermal annealing. Both suggest that thermal annealing promotes the

crystalline order in the PTB7-Th domains, preventing large changes in the $PC_{71}BM$ molecules positions.

With increased order, the $PC_{71}BM$ anions are better confined and the excess electrostatic potential energy after photon absorption is released by a more effective charge collection at the cathode from electrons coming from singlet character anions generated directly from singlet type excitons or from triplet type anions converted into singlets by thermal excitation. In keeping with this, thermally annealed electron-only DIO-free devices show an excellent stability against light-stress, as seen in **Figure 4**d, confirming that electron transport channels are not destructed by full sun illumination, once a high level of crystalline ordering in the $PC_{71}BM$ domains is achieved by the thermal treatment in DIO-free blends, as schematically depicted in Figure 1c.

### 2.4 Long-term stable PTB7-Th:$PC_{71}BM$ solar cells

To reach high performance long lifetime cells and to further reduce the burn-in effect without any significant reduction in performance, one may filter out high energy UV photons from a Xenon light source using a GG400 filter.[48] After re-calibration of the light intensity to 100 $mW/cm^2$ the cells exhibited an initial average PCE of 8.87% as indicated in **Table 1**. We monitored the performance of these cells under continuous light exposure up to 2300 h and, as shown in **Figure 5**, the cells retained more than 92% of their initial PCE. When we extrapolated the cell performance to later times by fitting a double exponential decay to the normalized PCE evolution measured (See Figure S12 in Supporting Information), we can predict a $T_{80}$ lifetime of more than 7 years assuming that 5.5 h of continuous full sun simulator illumination correspond to one day of outdoor light soaking. In contrast, as seen in

**Figure 5**, for the non-thermally treated PFN reference cells their performance dropped by more than 20% after 500 h of light soaking.

## 3. Conclusions

To summarize, our results demonstrate that in encapsulated devices, fully isolated form corrosive elements, the absorption of high energy photons by the electron transporting PCBM molecules leads to a degradation of exciton diffusion and charge mobility in the fullerene phase. Time resolved transient absorption measurements combined with UV wavelength cut-off degradation experiments indicate that the burn-in may be triggered by a spin flip at the donor/acceptor interface, creating PCBM anions of triplet type which result in the accumulation of electrostatic potential energy. This energy can only be dissipated through a disordering of the nano-morphology, mostly in the acceptor domains near the donor/acceptor interface. We propose a path to circumvent this problem by enhancing nano-crystalline ordering and its robustness, demonstrating that one may use high performance photovoltaic polymers and obtain very stable organic cells. We report that PTB7-Th cells, with an initial PCE close to 9%, exhibit T80 lifetimes as long as 7 years when under full sun light illumination. Provided that when left in the dark the encapsulated cells we fabricated suffer virtually no degradation, for the case of vertical applications in building integrated photovoltaics where sun irradiation is reduced by approximately a 0.67 factor (See Figure S13 in Support Information), the corresponding lifetime would be longer than 10 years. This is the longest lifetime ever reported for one sun illuminated polymer solar cells and may forge a way for the actual application of such technology. Finally, the route we provide to circumvent a degradation path intrinsic to the PCBM/polymer interface may lead to an increased stability applicable to any organic or hybrid technology that uses fullerene or PCBM derivatives as an electron-transporting layer or material.

## 4. Experimental Section

*Materials and preparation:* PTB7-Th and PFN from 1-material and electron acceptor $PC_{71}BM$ (purity > 99%) from American Dye Source were used as received. 0.3 M sol-gel ZnO precursor solutions and 1 mg/mL PFN solution were prepared according to previously reported method.[49,50] For binary solvent system, solutions of PTB7-Th: $PC_{71}BM$ (1.0:1.5 wt) at a concentration of 10 mg/mL were prepared in chlorobenzene (CB) and stirred at 60 $^{o}$C overnight in $N_2$-filled glovebox. Processing additive 1, 8-diiodoctane (3% vol) was added into the blends one hour prior to spin-coating. For DIO-free system, PTB7-Th: $PC_{71}BM$ (1:2, wt) at a concentration of 12 mg/mL were prepared in 1, 2-Dichlorobenzene (DCB) and stirred at 60 $^{o}$C overnight prior to spin-coating.

**Solar cell fabrication:** SG-ZnO based devices were fabricated by spin-casting ZnO sol-gel precursor on the pre-cleaned patterned ITO-coated glass substrates (Lumtec, 15 Ω/sq) and annealing at 180 $^{o}$C in air for 10 min to form a ~20 nm electron transporting layer. The prepared samples were then transferred into a $N_2$-filled glove box for spin-casting photoactive layer with a nominal thickness of ~100 nm. For PFN based devices, PFN solution was deposited on pre-cleaned ITO (without UVO or oxygen plasma treatment) in glovebox and annealed at 80 $^{o}$C for 5 min, followed by spin-casting photoactive layer with controlled thickness of ~100 nm. The resulting photoactive films were dried under high vacuum (< $5\times 10^{-7}$ mbar) for at least one hour. Finally, $MoO_3$ (8 nm) and Ag (150 nm) electrodes were sequentially deposited on the active layer through a shadow mask by thermal evaporation (< $5\times 10^{-6}$ mbar), which defines the active area of 0.06 $cm^2$. The deposition rate for $MoO_3$ and Ag was 0.5 Å /s and 1 Å/s, respectively. The devices were sealed with pre-cleaned glass and solvent-free ultraviolet curable epoxy (DELO KATIOBND LP655) in $N_2$-filled glovebox before measuring in air.

**Space-charge-limited current (SCLC):** SCLC measurements were performed on electron-only devices of ITO (135 nm)/SG-ZnO (20 nm)/blends (100 nm)/LiF (1 nm)/Al (100 nm) and hole-only devices of ITO (135 nm)/PEDOT: PSS (30 nm)/blends (100 nm)/$MoO_3$ (8 nm)/Ag (100 nm). The mobilities were extracted by fitting the *J*–V characteristics of single charge carrier devices using the SCLC Mott–Gurney model,[51,52] $J = \frac{9}{8}\varepsilon_r\varepsilon_0\mu_0\frac{(V\text{-}V_{bi})^2}{L^3}\exp(\beta\sqrt{\frac{V\text{-}V_{bi}}{L}})$, Where $\varepsilon_0$ is the permittivity of free space, $\varepsilon_r$ is the relative permittivity of the photoactive material (assumed to be 3.5), $V_{bi}$ is the built-in voltage (determined to be 0.1 V for the hole-only device and 0.1 V for the electron-only device), L is the thickness of the active layer , $\mu_0$ the zero-field mobility, and $\beta$ the field activation factor.

***Device characterization and Aging*:** *J*–V curves of all devices were measured with a Keithley 2420 source meter under a 1 sun, AM 1.5G spectrum from a solar simulator (ABET Sol3A, 1000 W/$m^2$). The illumination intensity of the light source (Xenon lamp, 300W, USHIO) was calibrated using a Hamamatsu silicon photodiode (with KG-5 filter, area=0.1296 $cm^2$) certificated by ISE Fraunhofer. Spectrally resolved EQEs were measured using a bench top QEX10 measurement system supplied by PV Measurements Inc. GIXD characterization of blend films on PFN-coated Si substrates was performed at beamline 7.3.3, Advanced Light Source (ALS), Lawrence Berkeley National Lab (LBNL). X-ray energy was 10 keV and operated in top off mode.[53] Transmission and absorption spectra were recorded with a Perkin Elmer Lambda 950 UV/vis spectrometer. For light stress tests, the samples were placed under solar simulator (ABET Sol3A) being continuously illuminated by one sun AM1.5G illumination in ambient air, except when taken out to carry out the *J*–V curve scans. The samples were left in open-circuit conditions between measurements. The temperature of the device surface during illumination was 40±5 °C as indicated by a thermocouple placed under the substrate. These ageing conditions correspond to the ISOS-L1 protocol.[54,55] For

post-thermal treatment, encapsulated devices were placed on a hotplate with controlled temperature of 85 ± 1 $^{o}$C and *J*–V characteristics were recorded when the cells cooled down to room temperature.

## Supporting Information

Supporting Information is available from the Wiley Online Library or from the author.

## Acknowledgements

We acknowledge financial support from the Spanish MINECO (Severo Ochoa program, grant No.: SEV-2015-0522), the MINECO and the Fondo Europeo de Desarrollo Regional FEDER (grant No.: MAT2014-52985-R), the Fundació Privada Cellex, and from the EC FP7 Program (ICT-2011.35) under grant agreement n° NMP3-SL-2013-604506, Q. L acknowledges Erasmus Mundus doctorate program Europhotonics (Grant No. 159224-1-2009-1-FR-ERA MUNDUS-EMJD). TPR was supported by supported by the U.S. Office of Naval Research under contract N00014-15-1-2244**.** Portions of this research were carried out at beamline 7.3.3 and 11.0.1.2 at the Advanced Light Source, which was supported by the DOE, Office of Science, and Office of Basic Energy Sciences.

Received: ((will be filled in by the editorial staff))
Revised: ((will be filled in by the editorial staff))
Published online: ((will be filled in by the editorial staff))

## References

[1] M. Jørgensen, K. Norrman, S. Gevorgyan, T. Tromholt, B. Andreasen, F. Krebs, *Adv. Mater*. **2012**, *24*, 580.

[2] D. F. Kronholm, J. C. Hummelen, Wiley: Weinheim, Germany, **2008**, pp 155.

[3] R. Chiechi, R. Havenith, J. Hummelen, L. Koster, M. Loi, *Mater. Today* **2013**, *16*, 281.

[4] R. Ganesamoorthy, G. Sathiyan, P. Sakthivel, *Sol. Energ. Mat. Sol. Cells*. **2017**, *161*, 102.

[5] K. Bush, A. Palmstrom, Z. Yu, M. Boccard, R. Cheacharoen, J. Mailoa, D. McMeekin, R. Hoye, C. Bailie, T. Leijtens, I. Peters, M. Minichetti, N. Rolston, R. Prasanna, S. Sofia, D. Harwood, W. Ma, F. Moghadam, H. Snaith, T. Buonassisi, Z. Holman, S. Bent, M. McGehee, *Nat. Energy* **2017** 2, 17009.

[6] F. Fu, T. Feurer, T. Weiss, S. Pisoni, E. Avancini, C. Andres, S. Buecheler, A. Tiwari, *Nat. Energy* **2016**, *2*, 16190.

[7] K. Baeg, M. Binda, D. Natali, M. Caironi, Y. Noh, *Adv. Mater.* **2013**, *25*, 4267.

[8] Y. Zheng, W. Liang, C. Xiong, Y. Yuan, Y. Chai, R. Yuan, *Anal. Chem.* **2016**, *88*, 8698.

[9] Y. Chen, H. Tian, J. Chen, Y. Geng, D. Yan, L. Wang, D. Ma, *J. Mater. Chem*. **2012**, *22*.8492.

[10] J. Hou, J. Wu, Z. Xie, L. Wang, *Appl. Phys. Lett.* **2009**, *95*, 203508.

[11] C. Peters, I. Sachs-Quintana, W. Mateker, T. Heumueller, J. Rivnay, R. Noriega, Z. Beiley, E. Hoke, A. Salleo, M. McGehee, *Adv. Mater.* **2011**, *24*, 663.

[12] D. Bartesaghi, G. Ye, R. Chiechi, L. Koster, *Adv. Energy Mater.* **2016**, *6*, 1502338.

[13] C. Schaffer, C. Palumbiny, M. Niedermeier, C. Jendrzejewski, G. Santoro, S. Roth, P. Müller-Buschbaum, *Adv. Mater.* **2013**, *25*, 6760.

[14] C. Schaffer, C. Palumbiny, M. Niedermeier, C. Burger, G. Santoro, S. Roth, P. Müller-Buschbaum, *Adv. Energy Mater.* **2016**, *6*, 1600712.

[15] M. Upama, M. Wright, B. Puthen-Veettil, N. Elumalai, M. Mahmud, D. Wang, K. Chan, C. Xu, F. Haque, A. Uddin, *RSC Adv.* **2016**, *6*, 103899.

[16] T. Heumueller, T. Burke, W. Mateker, I. Sachs-Quintana, K. Vandewal, C. Brabec, M. McGehee, *Adv. Energy Mater.***2015**, *5*, 1500111.

[17] L. Inasaridze, A. Shames, I. Martynov, B. Li, A. Mumyatov, D. Susarova, E. Katz, P. Troshin, *J. Mater. Chem. A* **2017**, *5*, 8044.

[18] T. Clarke, C. Lungenschmied, J. Peet, N. Drolet, K. Sunahara, A. Furube, A. Mozer, *Adv. Energy Mater.* **2013**, *3*, 1473.

[19] Y. Shao, Y. Yuan, J. Huang, *Nat. Energy* **2016**, *1*, 15001.

[20] S. Sapkota, M. Fischer, B. Zimmermann, U. Würfel, *Sol. Energ. Mat. Sol. Cells.* **2014**, *121*, 43.

[21] J. Jeong, J. Seo, S. Nam, H. Han, H. Kim, T. Anthopoulos, D. Bradley, Y. Kim, *Adv. Sci.* **2015**, *3*, 1500269.

[22] T. Leijtens, G. Eperon, S. Pathak, A. Abate, M. Lee, H. Snaith, *Nat. Commun.* **2013**, *4*, 2885.

[23] W. Mateker, M. McGehee, *Adv. Mater.* **2017**, *29*, 1603940.

[24] E. Yousif, R. Haddad, *SpringerPlus* **2013**, *2*, 398.

[25] Q. Liu, P. Mantilla-Perez, M. Montes Bajo, P. Romero-Gomez, J. Martorell, *ACS Appl. Mater. Interfaces* **2016**, *8*, 28750.

[26] G. Hedley, A. Ward, A. Alekseev, C. Howells, E. Martins, L. Serrano, G. Cooke, A. Ruseckas, I. Samuel, *Nat. Commun.* **2013**, *4*, 1038.

[27] F. Liu, W. Zhao, J. Tumbleston, C. Wang, Y. Gu, D. Wang, A. Briseno, H. Ade, T. Russell, *Adv. Energy Mater*. **2013**, *4*, 1301377.

[28] S. Liao, H. Jhuo, Y. Cheng, S. Chen, *Adv. Mater.* **2013**, *25*, 4766.

[29] Z. He, B. Xiao, F. Liu, H. Wu, Y. Yang, S. Xiao, C. Wang, T. Russell, Y. Cao, *Nat. Photon*. **2015**, *9*, 174.

[30] Y. Liang, Z. Xu, J. Xia, S. Tsai, Y. Wu, G. Li, C. Ray, L. Yu, *Adv. Mater.* **2010**, *22*, 135.

[31] B. Collins, Z. Li, J. Tumbleston, E. Gann, C. McNeill, H. Ade, *Adv. Energy Mater.* **2013**, *3*, 65.

[32] J. Kniepert, I. Lange, J. Heidbrink, J. Kurpiers, T. Brenner, L. Koster, D. Neher, *J. Phys. Chem. C* **2015** *119*, 8310.

[33] H. Kraus, M. Heiber, S. Väth, J. Kern, C. Deibel, A. Sperlich, V. Dyakonov, *Sci. Rep*.**2016**, *6*, 29158.

[34] A. Bakulin, S. Dimitrov, A. Rao, P. Chow, C. Nielsen, B. Schroeder, I. McCulloch, H. Bakker, J. Durrant, R. Friend, *J. Phys. Chem. Lett*. **2013**, *4*, 209.

[35] T. Clarke, J. Durrant, *Chem. Rev.***2010***, 110*, 6736.

[36] A. Distler, T. Sauermann, H. Egelhaaf, S. Rodman, D. Waller, K. Cheon, M. Lee, D. Guldi, *Adv. Energy Mater.* **2014**, *4*, 1300693.

[37] Z. Li, H. Wong, Z. Huang, H. Zhong, C. Tan, W. Tsoi, J. Kim, J. Durrant, J. Cabral, *Nat. Commun.***2014***, 4*,2227.

[38] Q. Burlingame, X. Tong, J. Hankett, M. Slootsky, Z. Chen, S. Forrest, *Energy Environ. Sci.* **2015**, *8*, 1005.

[39] T. Heumueller, W. Mateker, I. Sachs-Quintana, K. Vandewal, J. Bartelt, T. Burke, T. Ameri, C. Brabec, M. McGehee, *Energy Environ. Sci.* **2014**, *7*, 2974.

[40] T. Heumueller, W. Mateker, A. Distler, U. Fritze, R. Cheacharoen, W. Nguyen, M. Biele, M. Salvador, M. von Delius, H. Egelhaaf, M. McGehee, C. Brabec, *Energy Environ. Sci*. **2016***, 9*, 247.

[41] Q. Burlingame, B. Song, L. Ciammaruchi, G. Zanotti, J. Hankett, Z. Chen, E. Katz, S. Forrest, *Adv. Energy Mater*. **2016**, *6*, 1601094.

[42] J. Kong, S. Song, M. Yoo, G. Lee, O. Kwon, J. Park, H. Back, G. Kim, S. Lee, H. Suh, K. Lee, *Nat. Commun.* **2014**, *5*, 5688.

[43] W. Kim, J. Kim, E. Kim, T. Ahn, D. Wang, J. Park, *J. Phys. Chem. C* **2015**, *119*, 5954.

[44] W. Chang, L. Meng, L. Dou, J. You, C. Chen, Y. Yang, E. Young, G. Li, Y. Yang, *Macromolecules* **2015**, *48*, 562.

[45] P. Müller-Buschbaum, *Adv. Mater.* **2014**, *26*, 7692.

[46] J. Rivnay, S. Mannsfeld, C. Miller, A. Salleo, M. Toney, *Chem. Rev*. **2012**, *112*, 5488.

[47] F. Liu, Y. Gu, X. Shen, S. Ferdous, H. Wang, T. Russell, *Prog. Polym. Sci.* **2013***, 38*, 1990.

[48] Z. Ding, J. Kettle, M. Horie, S. Chang, G. Smith, A. Shames, E. Katz, *J. Mater. Chem. A* **2016**, *4*, 7274.

[49] D. Ghosh, Q. Liu, P. Mantilla-Perez, T. Chen, V. Mkhitaryan, M. Huang, S. Garner, J. Martorell, V. Pruneri, *Adv. Funct. Mater*. **2015**, *25*, 7309.

[50] X. Elias, Q. Liu, C. Gimbert-Suriñach, R. Matheu, P. Mantilla-Perez, A. Martinez-Otero, X. Sala, J. Martorell, A. Llobet, *ACS Catalysis* **2016**, *6*, 3310.

[51] C. Melzer, E. Koop, V. Mihailetchi, P. Blom, *Adv. Funct. Mater.* **2014**, 14, 865.

[52] V. Vohra, K. Kawashima, T. Kakara, T. Koganezawa, I. Osaka, K. Takimiya, H. Murata, *Nat. Photon*. **2015**, *9*, 403.

[53] L. Nian, K. Gao, F. Liu, Y. Kan, X. Jiang, L. Liu, Z. Xie, X. Peng, T. Russell, Y. Ma, *Adv. Mater*. **2016**, *28*, 8184.

[54] M. O. Reese, S. A. Gevorgyan, M. Jørgensen, E. Bundgaard, S. R. Kurtz, D. S. Ginley, D. C. Olson, M. T. Lloyd, P. Morvillo, E. A. Katz, A. Elschner, O. Haillant, T. R. Currier, V. Shrotriya, M. Hermenau, M. Riede, K. R. Kirov, G. Trimmel, T. Rath, O. Inganäs, F. Zhang, M. Andersson, K. Tvingstedt, M. Lira-Cantu, D. Laird, C. McGuiness, S. J. Gowrisanker, M. Pannone, M. Xiao, J. Hauch, R. Steim, D. M. DeLongchamp, R. Rösch, H. Hoppe, N. Espinosa, A. Urbina, G. Yaman-Uzunoglu, J. Bonekamp, A. J. J. M. van Breemen, C. Girotto, E. Voroshazi, F. C. Krebs, *Sol. Energy Mater. Sol. Cells* **2011**, *95*, 1253.

[55] R. Roesch, T. Faber, E. von Hauff, T. Brown, M. Lira-Cantu, H. Hoppe, *Adv. Energy Mater.* **2015**, *5*, 1501407.

**Table 1**. PV parameters of inverted ITO/PFN/PTB7-Th:$PC_{71}BM$/$MoO_3$/Ag devices fabricated with different solvent under AM 1.5G solar illumination at 1000 $Wm^{-2}$ and lifetimes.

| Solar cell type | | $J_{sc}$ (mA $cm^{-2}$) | $V_{oc}$ (V) | *FF* (%) | *PCE* (%)[a] | $A_1$ | $T_{80}$ ( h) [b] |
|---|---|---|---|---|---|---|---|
| ZnO-reference | Fresh | 16.85 ± 0.15 | 0.801 ± 0.009 | 70.27 ± 0.53 | 9.49 ± 0.12 (9.72) | 0.7985 | <1 |
| DIO-free | Fresh | 16.01±0.22 | 0.802 ± 0.002 | 72.28 ± 0.78 | 9.28 ± 0.17 (9.59) | 0.7537 | ~ 4 |
| DIO-free | 85 °C/ 25 h | 15.70 ± 0.32 | 0.815 ± 0.001 | 68.65 ± 0.50 | 8.87 ± 0.19 (9.07) | 0.0628 | ~1500 |
| | | | | | | 0.0327[c] | ~ 14250[c] |

[a]. The average values and standard deviations are obtained over 10 devices and the best PCE values are shown in parentheses.

[b]. Lifetime $T_{80}$ is the time for PCE to degrade to 80% of the initial value, which is determined by fitting normalized PCE evolutions under AM1.5G 1-sun illumination using a double-exponential decay function $PCE\ (t)=A_1 \cdot exp(-t/\tau_1)+ A_2 \cdot exp(-t/\tau_2)$[44], where $A_1$ and $A_2$ are the amplitudes for each exponential function. $\tau_1$ and $\tau_2$ are the respective lifetime constants of the exponential decays.

[c]. $A_1$ and $T_{80}$ are derived from normalized PCE decay under UV-filtered AM1.5G (GG400, $\lambda >$ 400 nm) 1-sun illumination.

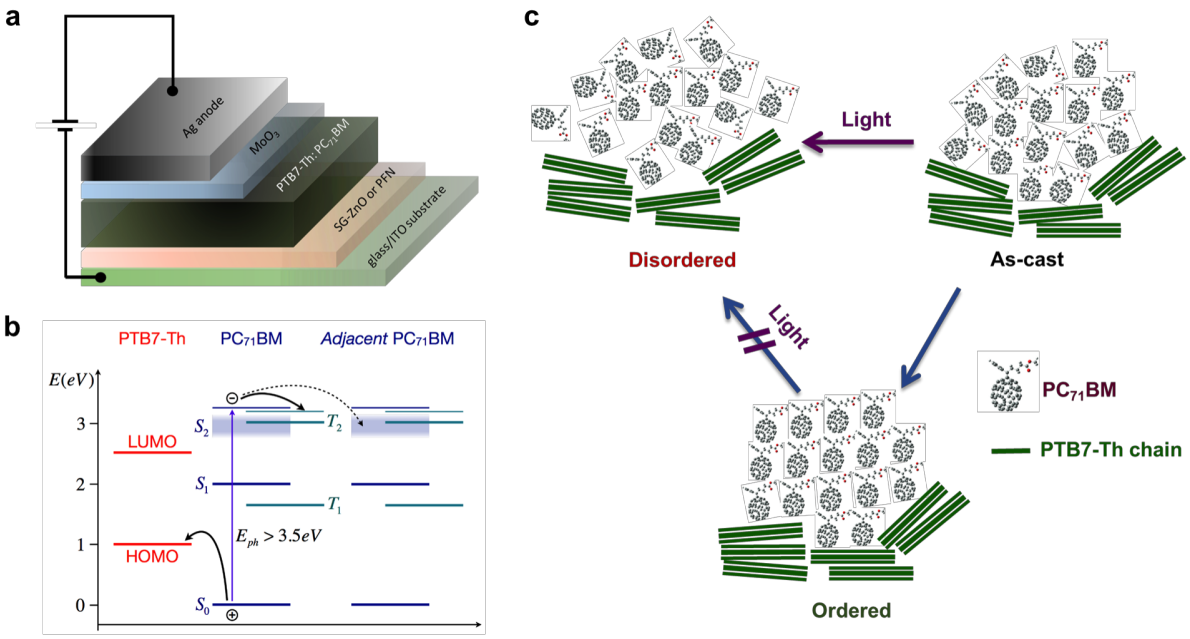


**Figure 1.** Device architecture and degradation mechanism. **a**) Device structure of the inverted polymer solar cells in this study: ITO/SG-ZnO or PFN/PTB7-Th:$PC_{71}BM$/$MoO_3$/Ag anode. Here, PFN is Poly[(9,9-bis(3'-(N,N-dimethylamino)propyl)-2,7-fluorene)-alt-2,7-(9,9 dioctylfluorene)], PTB7-Th is poly [[2,6-4,8-di(5-ethylhexylthienyl)benzo[1,2-b;3,3-b]dithiophene][3-fluoro-2[(2-ethylhexyl)carbonyl] thieno[3,4-b]thiophenediyl]] and $PC_{71}BM$ is [6,6]-phenyl $C_{71}$-butyric acid methyl ester. **b**) Schematic illustration of the relevant electronic states in PTB7-Th:$PC_{71}BM$ blends. $PC_{71}BM$ ground states ($S_0$), singlet excited states ($S_1$ and $S_2$), and triplet states ($T_1$ and $T_2$) are indicated. Two possible paths for electrons in the acceptor domains after the splitting of high energy excitons are indicated. **c**) Schematic drawing of two possible paths for the nano-morphology evolution in the $PC_{71}BM$ acceptor phase: in the top one light induces disorder and in the bottom one light induced disorder is prevented in a highly crystalline configuration of the $PC_{71}BM$ molecules.

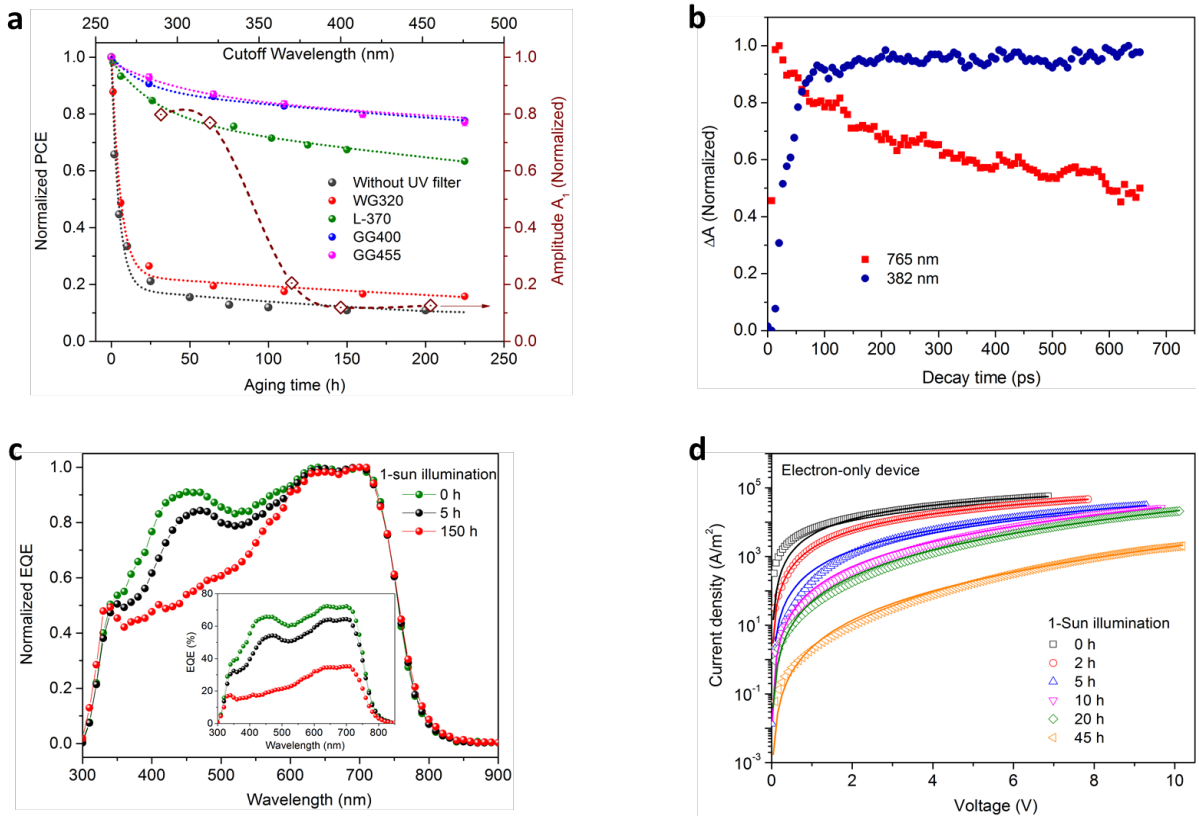


**Figure 2.** UV-induced degradation in PTB7-Th:$PC_{71}BM$ blends. **a**) Left and bottom axes: normalized experimental PCE evolutions (solid dots) under a UV filtered AM 1.5G 1-sun illumination and solid lines present the best double-exponential decay fittings. Top and right axes: Normalized amplitude for the first exponential in terms of the cut-off wavelength of the filer used. The cut-off wavelength of the long-pass UV filters is indicated dependent. **b**) Transient absorption measurements on glass/PTB7-Th:$PC_{71}BM$ films prepared from reference blends. **c**) Normalized external quantum efficiency (EQE) evolution under AM 1.5G 1-sun illumination. Inset: Absolute EQE spectra evolution. **d**) Semi-log plot of the *J*–V characteristics for the ITO (135 nm)/SG-ZnO (20 nm)/PTB7-Th:$PC_{71}BM$ (CB+3%DIO, 100 nm)/LiF (1 nm)/Al (100 nm) electron-only devices with respect to aging time under non-UV-filtered AM 1.5G illumination at 100 $mWcm^{-2}$. The solid lines present the best fittings using the SCLC modified Mott–Gurney model.

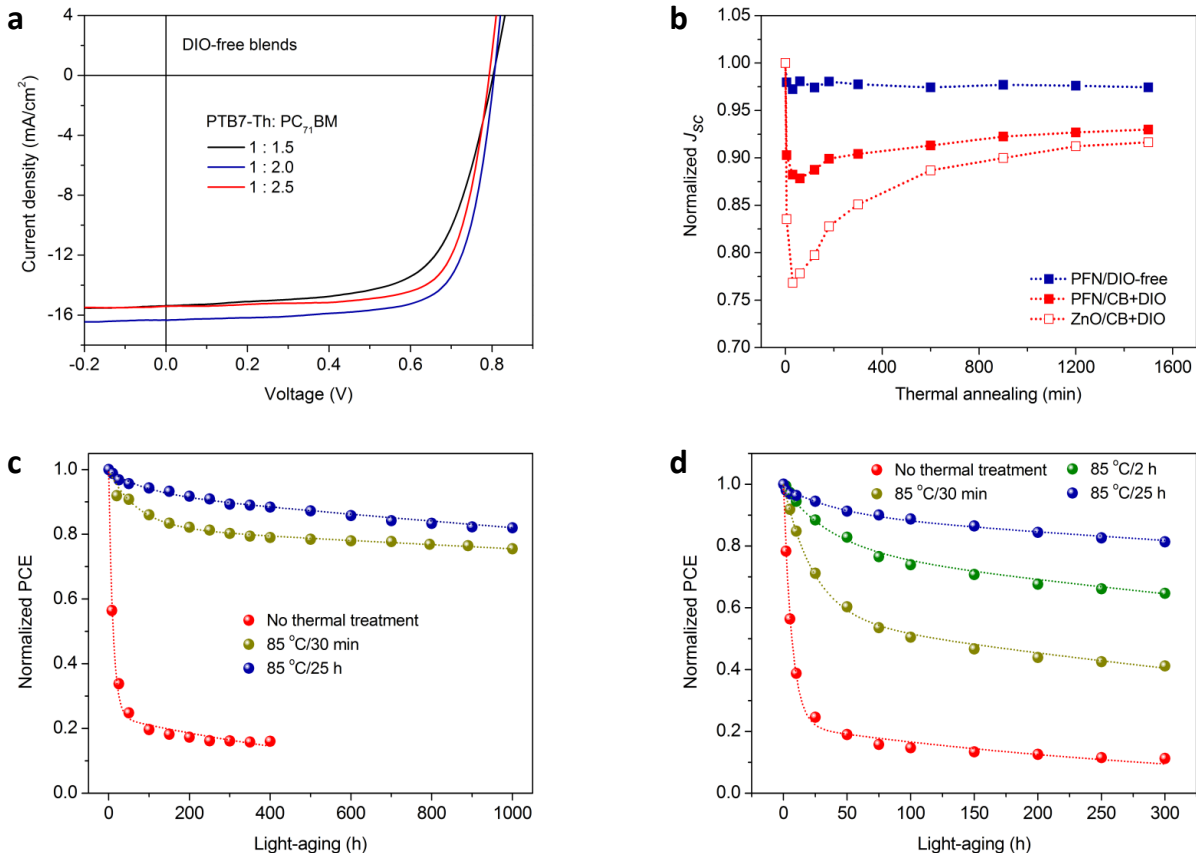


**Figure 3. a**) *J*–V curves for DIO-free cells with various PTB7-Th:$PC_{71}BM$ ratios. **b)** Normalized $J_{sc}$ evolution for ZnO reference, PFN reference and DIO-free devices during a 25 h of thermal annealing at 85 °C in air and room light. **c**) Normalized PCE evolution under non-UV-filtered AM 1.5G 1-sun illumination of DIO-free devices for three different thermal annealing times. **d**) Normalized PCE evolution for PFN reference devices under non-UV-filtered AM 1.5G 1-sun illumination for four different thermal annealing times.

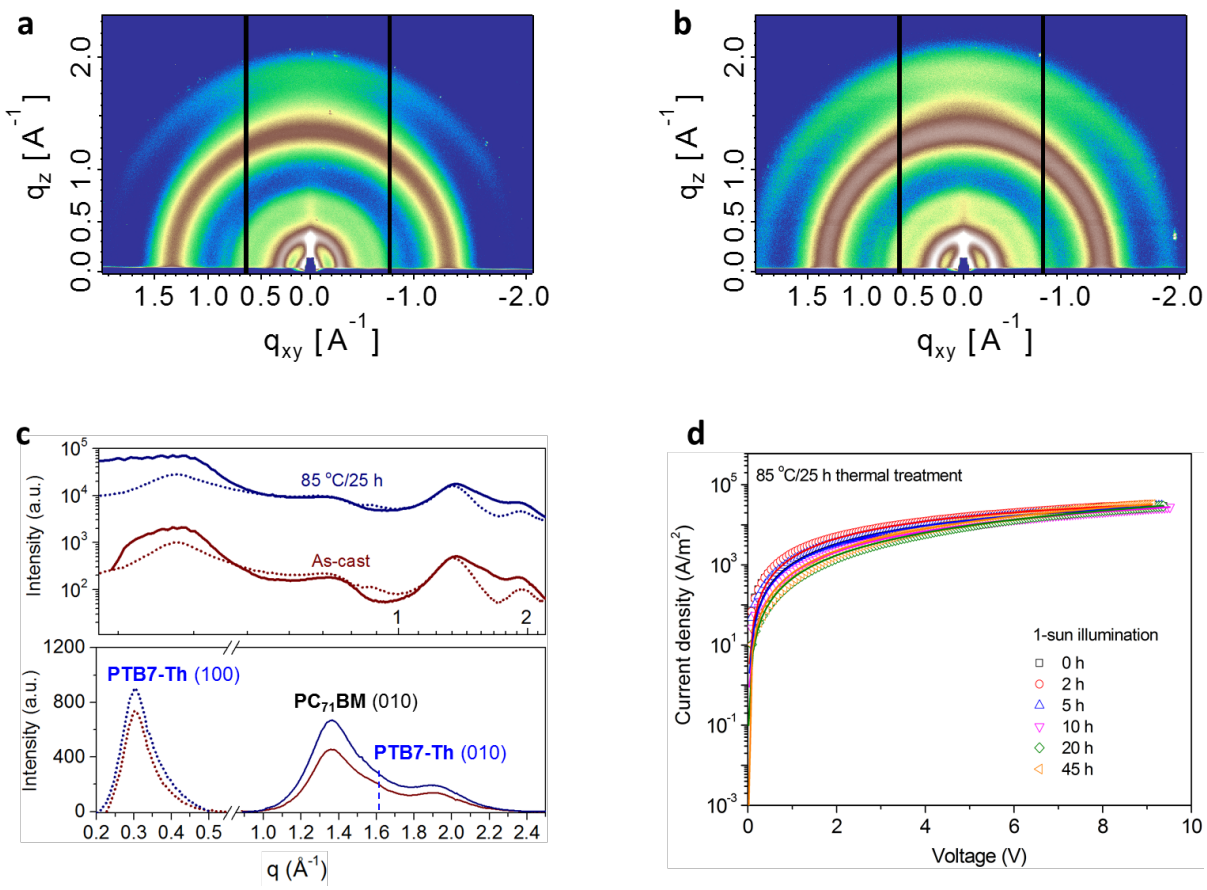


**Figure 4.** Crystalline morphology in $PC_{71}BM$ phase. Two-dimensional GIXD patterns of the Si substrate/PFN/DIO-free active layer (**a**) without annealing and (**b**) with 25 h thermal annealing in $N_2$-filled glovebox. **c**) Top: 1-D in-plane (dotted lines) and out-of-plane (solid lines) X-ray line-cut profiles extracted from GIXD and bottom: line-cut profiles after subtracting the baseline. **d**) *J*–V evolution of 25 h thermally annealed ITO (135 nm)/PFN (10 nm)/PTB7-Th:$PC_{71}BM$ (DIO-free, 100 nm)/LiF (1 nm)/Al (100 nm) electron-only devices under non-UV-filtered AM 1.5G illumination at 100 $mWcm^{-2}$.

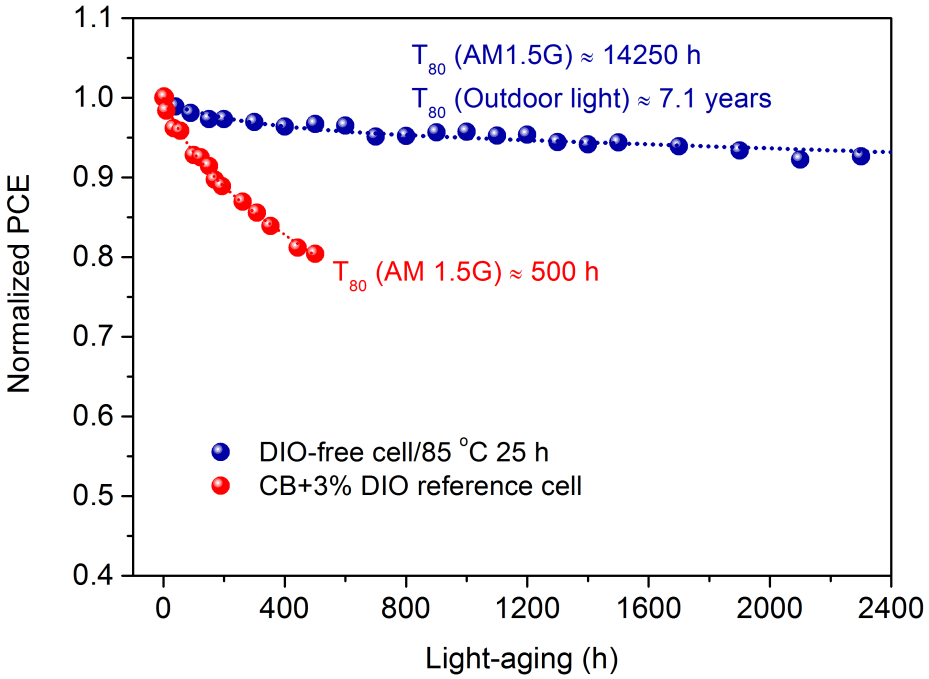


**Figure 5.** High performance long lifetime PTB7-Th: $PC_{71}BM$ solar cells. Experimental (solid dots) and double exponential decay fittings (dashed lines) of normalized PCE evolutions for a 25 h thermally annealed DIO-free (blue) and a PFN reference (red) cells under a continuous UV-filtered ($\lambda >$ 400 nm) AM 1.5G illumination at 100 $mWcm^{-2}$. Each point represents the average over six individual cells.

**The table of contents**.

A spin flip at the donor/acceptor interface is demonstrated after absorbing high energy photons, leading to the accumulation of electrostatic potential energy that initiates a rapid destruction of the fullerene nano-morpholgy in polymer cells. By inducing a robust nano-crystalline ordering in the $PC_{71}BM$, a high performance (~9%) and long lifetime (~10 years) solar cell is obtained.

**Keywords:** Organic photovoltaics, photostability, PCBM, PTB7-Th, Burn-in

Dr. Q. Liu[1], Dr. J. Toudert[1], Prof. F. Liu[2,3], Dr. P. Mantilla-Perez[1], Dr. M. M. Bajo[1], Prof. T. P. Russell[4] and Prof. J. Martorell[1,5]*

**Title: Circumventing spin flip induced nano-morphology disorder to achieve long lifetime PCBM based solar cells**